PAPER

Check for updates

Tuning residual chirality in carbon dots with anti-microbial properties†

Florence Victoria,[abc] John Manioudakis,[abc] Liana Zaroubi,[a] Brandon Findlay[a] and Rafik Naccache [ID] *[abc]

Chirality remains a critical consideration in drug development and design, as well as in applications of enantioselective recognition and sensing. However, the preparation of chiral nanomaterials requires extensive post synthetic modifications with a chiral agent, coupled with extensive purification. This limits the use and application of chiral nanomaterials. Herein, we report a facile, one-step microwave-assisted synthesis of chiral carbon dots through the reaction of L- and D-cysteine amino acid precursors and citric acid. We modulated the synthetic parameters to preserve and tune the residual chiral properties of the dots and demonstrate that the reaction conditions play a critical role in dictating the chiral behaviour of the dots. Finally, in a proof of concept application we demonstrated that the synthesized carbon dots, particularly D-carbon dots inhibit bacterial growth at a lower concentration than L-carbon dots. By varying bacterial strains and chirality of the carbon dots, concentrations ranging from $0.25-4$ mg mL^{-1} of the nanoparticles were required to inhibit microbial growth. The ability to preserve and tune chirality during synthesis can open up novel avenues and research directions for the development of enantioselective materials, as well as antibacterial films and surfaces.

Introduction

Nature is comprised of homochiral materials and molecules. Indeed, all living systems are made up of chiral L-amino acids, enzymes and proteins, as well as D-sugars in the backbones of DNA and RNA. In achiral environments, enantiomers are known to interact identically; however, in chiral environments, these compounds distinctively interact with their surroundings due to high stereospecificity. As such, chirality contributes a fundamental role in biochemical recognition including smell and taste, in chemical communication, in signalling pathways and in enzymatic reactions.[1] Moreover, in the pharmaceutical industry, over 50% of the drugs exist as chiral compounds where only one of the enantiomer exhibits the desired pharmacological activity while the other enantiomer often has adverse effects, or reduced efficacy.[2–4]

Chirality has also garnered increasing interest in the field of nanomaterials for applications such as asymmetrical catalysis, enantioselective recognition, and chiral sensing. Several chiral nanomaterial systems have been reported in the literature ranging from inorganic metallic nanoparticles,[5–8] semi-conductors[9–13] and mesoporous silica,[14–17] to organic nano-structures such as polymers,[18–20] among others. Chirality has also been explored in carbon-based nanoparticles such as fullerenes,[21] carbon nanotubes[22–24] and graphene dots.[25–27] More recently, chirality has been investigated in carbon dots (CD), one of the more recent members of the carbon allotrope family. CDs are ~10 nm in size and are quasi-spherical. Typically, they are comprised of predominantly sp^2 conjugated hybridized carbons with some sp^3 character. They are mainly composed of carbon, oxygen, nitrogen and hydrogen, but may be doped with other heteroatoms (*e.g.* sulfur) depending on the chemical composition of the starting materials.[28–30] The emerging interest in chiral carbon dots stems from the fact that their synthesis can be both sustainable and cost efficient coupled with the fact that their physico-optical properties can be tailored during synthesis. CDs are highly dispersible in water, have high resistance to photo-bleaching, as well as low cytotoxicity and high biocompatibility.

It is in this regard that they have been touted as excellent candidates for applications in sensing, bioimaging and nano-medicine,[31,32] among others. One of the first chiral CDs reported in the literature was synthesized by Ghosh *et al.* from the nucleotide guanosine 5′-monophosphate, where these G-dots were capable of intrinsically self-assembling to form biode-gradable chiral hydrogels which could be used for biomedical applications and drug delivery.[33] Zhang *et al.* also synthesized chiral CDs through hydrothermal synthesis by using L- and

aDepartment of Chemistry and Biochemistry, Concordia University, Montreal, QC, Canada, H4B 1R6. E-mail: rafik.naccache@concordia.ca

bCentre for NanoScience Research, Concordia University, Montreal, QC, H4B 1R6

cQuebec Centre for Advanced Materials, Department of Chemistry and Biochemistry, Concordia University, Montreal, QC, H4B 1R6, Canada

† Electronic supplementary information (ESI) available. See DOI: 10.1039/d0ra05208f

D-cysteine with citric acid. These CDs were explored as electrochemical probes for enantioselective recognition towards small target molecules such as enantiomeric tartaric acid, through a combination of electrochemical impedance spectroscopy (EIS) and linear sweep voltammetry.[34] Deka *et al.* reported chiral CDs from an array of chiral amino acids and they studied the different chiral interactions with photosensitizers under UV radiation.[35] Chiral CDs in biological systems have also been explored, as in the work of Hu *et al.* who synthesized CDs from enantiomers of cysteine.[36] They investigated the activity of laccase enzyme under the influence of chiral CDs.[36] Similarly, chiral cysteine-based CDs were used by Li *et al.* to understand its influence on cellular energy metabolism[37] and by Zhang *et al.* to study its effects on mung bean plant growth.[38] While these studies have provided a wealth of information on the properties of chiral CDs, many questions remain unanswered. In particular, (i) how chirality varies when starting with D- *vs.* L-enantiomers, or a mixture of both, (ii) whether these CDs are indeed chirally-distinct from the precursor molecules and (iii) how the chiral building blocks come to form CDs, and the nature of the intermediate molecules that polymerize and carbonize to produce the complete chiral nanoparticle.

Herein, we report a facile one-step microwave-assisted synthesis of chiral CDs from the chiral amino acid cysteine and achiral citric acid. We tuned the residual chirality observed in our CDs by controlling reaction parameters including temperature, time and chiral precursor concentration. We also unequivocally demonstrated that the observed chirality is clearly distinct from the chiral precursors and finally, in a proof of concept application, we demonstrated that these chiral carbon dots have antimicrobial activity, inhibiting the growth of various strains of Gram-negative and Gram-positive bacteria. This antimicrobial activity was also retained when the CDs were impregnated in an agar surface, suggesting that they may serve as potential antimicrobial additives in smart surfaces.

Experimental

Materials

All chemicals were used as purchased without further purification. L- and D-cysteine ($C_3H_7NO_2S$), and citric acid ($C_6H_8O_7$) were all purchased from Sigma Aldrich. Milli-Q water was produced in-house. All reagents were of analytical grade and were used as is, without the need for further purification.

Methods

Synthesis of chiral carbon dots. The CDs were synthesized in a one-step microwave reaction with citric acid, the chiral amino acid and water. A 2 mL solution of equimolar citric acid and amino acid precursor was heated in a 10 mL microwave vial at temperatures ranging from 160 °C to 220 °C for a duration of time ranging from 5–15 min. The CDs were purified from unreacted precursors and fluorophores through dialysis using 1 kDa MWCO dialysis bags (Spectra/Por®6 RC – Spectrum Laboratories), then concentrated down by evaporation and finally washed with acetone and centrifuged at room temperature at

$10\ 000 \times g$ for 10 min. The supernatant was discarded, and the pellet was washed until no fluorescence was observed in the supernatant. The pellet was dried to produce a brown powder in a 70 °C oven and then resuspended in water for further analysis. The reaction conditions of the synthesis for all CDs are summarized in the ESI (Table S1†).

Transmission electron microscopy (TEM). For Transmission Electron Microscopy (TEM), CDs were dispersed in water at a concentration of 100 μg mL^{-1} solution and applied to the formvar-coated 200 mesh copper TEM grids (Electron Microscopy Sciences).

Absorbance spectroscopy. UV-visible absorption spectra were obtained in the spectral range of 200–800 nm using a Cary 5 Series UV-Vis-NIR Spectrophotometer (Agilent Technologies). A 1 cm quartz cuvette was used with a 2.5 nm bandwidth and wavelength changeover at 400 nm. All data collection and processing were carried out with an Agilent Cary Eclipse Scan software package.

Fluorescence spectroscopy. Fluorescence spectra were recorded using a Cary Eclipse Fluorescence Spectrophotometer (Agilent Technologies). The concentration of the CDs dispersed in water were adjusted to an absorbance value of 0.1 a.u. to minimize inner filter effects. Spectra were acquired in a 1 cm quartz cuvette at λ_{ex} = 250–550 nm (100 nm intervals). The excitation and emission slits were set to a width of 2.5 nm with a PMT voltage at 600 V. All data were processed using the Agilent Cary Eclipse application software.

Fourier transform infrared spectroscopy-attenuated total reflectance (FTIR-ATR). Fourier-Transform Infrared Spectroscopy (FT-IR) spectra were collected using a Thermo Scientific Nicolet iS5 equipped with an iD5 ATR accessory. Spectra were collected using 64 scans with a resolution of 0.4 cm^{-1}, a gain of 1, an optical velocity 0.4747 and an aperture setting of 100. Data was processed using the Thermo Scientific Nicolet Omnic 9 software.

X-ray photoelectron spectroscopy (XPS). X-ray Photoelectron Spectroscopy (XPS) spectra of the CDs were acquired using a Thermo Scientific K-Alpha X-ray Photoelectron Spectrometer. A total of 10 scans were collected per analysis and repeated in triplicate. The analysis was done using the Thermo Scientific™ Avantage Data System software.

Circular dichroism. Circular dichroism spectra were obtained using a JASCO J-815 spectropolarimeter (JASCO) and a 10 mm quartz cuvette. The data was collected from 180 nm to 500 nm in 3 accumulations. The scans were continuous with a scanning speed of 50 nm min^{-1}. The data was processed using Spectra Manager II software.

Thermogravimetric analysis (TGA). TGA analysis was conducted on powdered CDs using TGA-Q500 from TA Instruments in platinum pans, under a nitrogen environment. The samples were heated at a rate of 10 °C min^{-1} from 30 °C to 1000 °C and the data was analyzed using the Thermal Advantage 5.0 software.

Bacterial cultivation. *Escherichia coli* ATCC 25922 and *Klebsiella aerogenes* ATCC 13048 were acquired from the American Type Culture Collection (ATCC). *E. coli* MG1655 and *B. thailandensis* E264 were obtained from Prof. Eric Déziel, INRS-

Institut Armand Frappier. *M. luteus* DSM20030 and *B. subtilis* DSM10 were obtained from the Leibniz Institute DSMZ-German Collection of Microorganisms and Cell Cultures. Bacteria were grown in Luria–Bertani (LB) media, at either 37 °C (*E. coli*) or 30 °C (*M. luteus*, *B. subtilis*, *B. thailandensis*, *K. aerogenes*), rotating at 225 rpm. Bacterial isolates were streaked on 1.5% agar LB plates and placed at 37 °C or 30 °C for 18–24 hours prior to MIC testing.

MIC determinations. Following CLSI guidelines for broth microdilution and direct colony suspension testing,[39] bacterial cultures were transferred to Mueller–Hinton broth (MHB) (*E. coli*) or LB (*M. luteus*, *B. subtilis*, *B. thailandensis*, *K. aerogenes*) and adjusted to a final turbidity equivalent to a 0.5 McFarland standard (1.5×10^8 CFU mL^{-1}). Bacteria were diluted to 1.5×10^6 CFU mL^{-1} then mixed 1 : 1 with the compound of interest in 96-well plates, then incubated at 30 °C for 20–24 hours (*M. luteus*, *B. subtilis*, *B. thailandensis*, *K. aerogenes*) or 37 °C (*E. coli*) for 16–20 hours (all other strains). The minimum inhibitory concentration (MIC) was defined as the concentration sufficient to inhibit bacterial growth as measured by the naked eye. For MIC testing in solid agar *E. coli* was adjusted to 1×10^6 CFU mL^{-1} in MHB, then streaked onto MHA laced with the noted concentration of L- or D-cysCDs. As with the broth microdilutions, plates were placed at 37 °C for 16–20 hours prior to MIC determination as per CLSI guidelines.[40]

Results and discussion

Chiral cysteine CDs (L-cysCDs or D-cysCDs) were synthesized *via* an aqueous microwave reaction using citric acid as the principal carbon source in conjunction with L- and D-cysteine. The microwave synthesis of chiral CDs allowed for a simple, rapid, and efficient procedure in comparison to other methods. Furthermore, it allowed for precise control and monitoring of reaction parameters such as temperature, time and pressure throughout the synthesis. Following an extensive purification to remove any unreacted precursors, the CDs remained well-dispersed in water or other polar solvents such as methanol and did not display any agglomeration over a period of several

weeks. The aim of our work was to examine how the residual chirality of the cysCDs can be controlled by varying the reaction parameters including time, temperature and starting material concentration. Indeed, CDs have been known to form *via* a series of condensation reactions that generate fluorophores, which subsequently polymerize and carbonize to form the dots. In our system, the chirality originates from the chiral cysteine molecules, which react with the citric acid to form intermediates like 5-oxo-3,5-dihydro-2*H*-thiazolo[3,2-*a*]pyridine-3,7-dicarboxylic acid (TPDCA).[41,42] These intermediates undergo polymerization reaction between several units followed by carbonization reactions to form the nanoparticles. Since the reaction parameters are known to play a critical role in the formation of the CDs, it would thus be expected to impact the residual chiral signal along with the optical properties of the dots.

The optical properties of the L- and D-cysCDs, prepared at a temperature of 160 °C with a 10 min reaction time and a 1 : 1 concentration of citric acid to L-/D-cysteine precursor, were characterized using UV-Vis, fluorescence and circular dichroism spectroscopies (Fig. 1). The UV-Vis spectra (Fig. 1a) of the chiral CDs revealed two distinct absorption bands centred at ~250 nm and ~350 nm. The former absorbance band is characteristic of the $\pi \rightarrow \pi^*$ transition of the aromatic sp^2 domains, while the latter is attributed to the n $\rightarrow \pi^*$ transitions of the C=O, as well as the C=N/C=S bonds of the aromatic CD core. As expected, both L- and D-cysCDs show similar absorbance profiles since they are comprised of enantiomers of the same precursors.

The cysCDs dispersed in water, at working concentrations of approximately 10 μg mL^{-1}, exhibited an intense blue emission easily visualized by the naked eye under UV light ($\lambda_{ex} = 365$ nm) (Fig. 1b inset). The enantiomers of the cysCDs show an emission maximum at 420 nm following 350 nm excitation wavelength by fluorescence spectroscopy with minimal difference in their profiles (Fig. 1b). The cysCDs exhibited an excitation independent emission with an increasing excitation wavelength. A control experiment of the unpassivated carbon dots, using only citric acid as the precursor, was also conducted. These unpassivated carbon dots had an absorption band
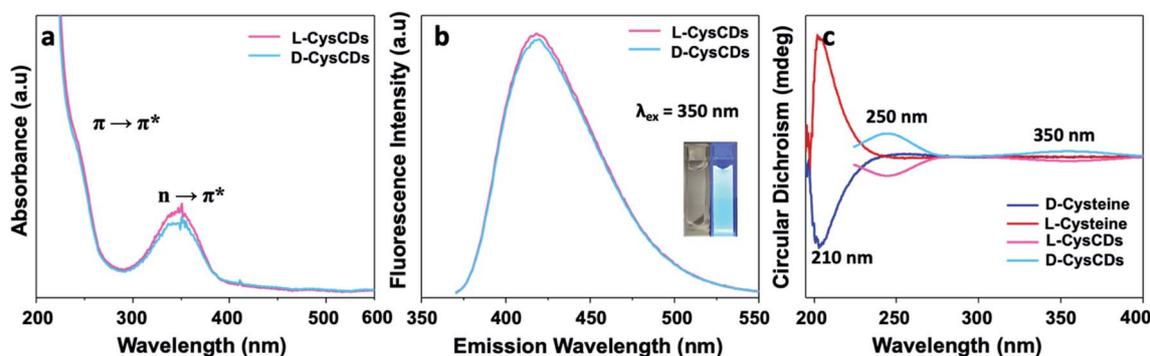

Fig. 1 Optical characterization of chiral cysCDs. (a) Absorbance spectra of L- and D-cysCDs show identical absorbance bands at 250 nm for the $\pi \rightarrow \pi^*$ and at 350 nm for the n $\rightarrow \pi^*$. (b) Fluorescence analysis of L- and D-cysCD evidence similar profiles following $\lambda_{ex} = 350$ nm. The inset image shows cysCDs under laboratory neon lights in the left panel and in the right panel the same solution is excited using a 365 nm UV lamp. (c) The chirality of L- and D-cysCDs in comparison to the L and D-cysteine precursors show clearly distinct absorption bands.

centred at ~350 nm (Fig. S1a†) and no significant fluorescence was observed highlighting the importance of functional groups in increasing radiative pathways (Fig. S1b†).

The observed optical properties are in accordance with other cysteine based chiral CDs, prepared using hydrothermal synthesis.[33–38] The prominent peaks of the previously reported hydrothermal cysteine-based CDs were also centred around ~250 nm and ~350 nm. The similarities in optical properties of CDs from the two different synthesis methods can be attributed to the use of the same precursors with similar resulting functional groups and properties. The hydrothermal and microwave-prepared CDs also evidence excitation independent photoluminescence; however, the hydrothermal preparation approach resulted in CDs with an emission maximum at ~520 nm. This could be due to the differences in size of the dots prepared using the two preparation methods.

Following absorbance and fluorescence characterization, circular dichroism spectroscopy was used to investigate whether the cysCDs prepared from the chiral L- or D-precursors had retained any chirality. L- and D-cysCDs show prominent absorbance bands at 250 nm and 350 nm equal in magnitude but opposite in sign. These bands are significantly different from the cysteine precursors, which show a single absorbance at approximately 210 nm (Fig. 1c). L-Cysteine gives rise to L-cysCDs and D-cysteine gives rise to D-cysCDs respectively and both sets of chiral L- and D-cysCDs, prepared under the same experimental conditions, display a highly symmetrical interaction with circularly polarized light and show a mirror image response. The peaks at 250 nm and 350 nm are equivalent to previous studies that have synthesized chiral cysCDs

and they correspond to the UV-Vis absorbance bands of the dots.[34–38] Furthermore, the unpassivated carbon dots composed of citric acid did not display any absorbance bands in the circular dichroism spectra (Fig. S1c†).

The physical characteristics of the cysCDs were thoroughly investigated to glean an understanding of their physico-chemical and optical properties. Transmission electron microscopy (TEM) analysis of the cysCDs shows an average nanoparticle size of 12 ± 3 nm (Fig. 2a). The cysCDs were quasi-spherical with a Gaussian size distribution ranging from 6–28 nm over a large population of the chiral CDs. The TEM images and the size distributions of cysCDs prepared at various reaction parameters are summarized in the ESI (Table S2 and Fig. S2–S5†). The amorphous nature of the CDs was examined using X-ray diffraction spectroscopy (XRD) and the cysCDs depicted the expected amorphous halo centred at ~17° 2θ with the presence of several sharp crystalline peaks located at 21, 30, 31, 33 and 35° 2θ (Fig. S6†). The halo is typically associated with the (002) plane of graphene[43,44] while the sharp features in the XRD suggests possible ordered semi-crystalline regions in the nanoparticle.

Additionally, the cysCDs were also analysed using thermogravimetric analysis (TGA) to further investigate their composition and study their thermal stability, which differ from the citric acid and the cysteine precursor (Fig. S7†). TGA indicates that there is 2% loss upon heating from 30–100 °C and a 5% loss from 100–150 °C. This was attributed to residual moisture and solvent adsorbed on the surface following synthesis and purification procedures. The large weight loss of 58% is noted between 200–500 °C and is ascribed to decomposition of the
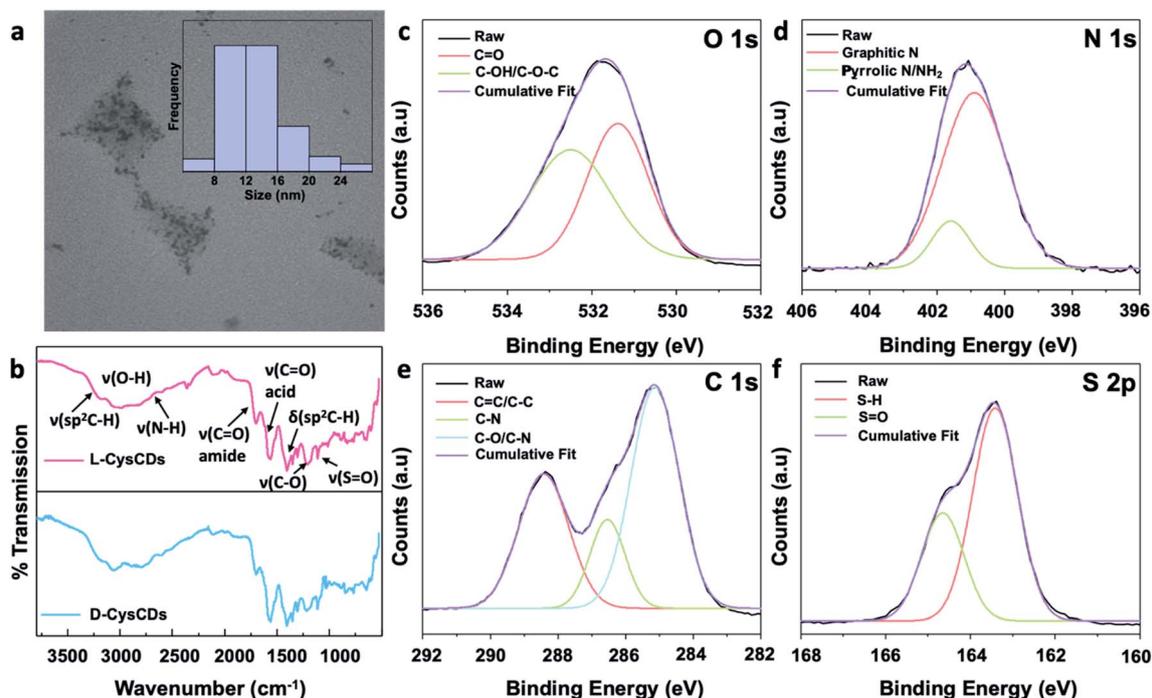

Fig. 2 Physical characterization of the chiral cysCDs. (a) TEM image of the cysCDs depicts quasi-spherical nanoparticles with an average size of 12 ± 3 nm, (b) FTIR spectra of L- and D-cysCDs indicates that the surface functional groups present on the CDs are comprised of amino, carboxylic acid and other oxygen-containing functional groups, (c–f) High resolution XPS spectra of cysCDs also indicates the presence of amino, carboxylic, oxygen and sulfur containing moieties.

functional groups on the surface. Typically, oxygen, nitrogen and sulphur containing moieties undergo decomposition at such a temperature range.[45–47] The weight loss occurring past 500 °C corresponds to oxidation of the amorphous carbon that forms the nanoparticle core.

As the properties of the nanoparticles were determined by their composition, the cysCDs were characterized by Fourier Transform Infrared (FT-IR) and X-ray photoelectron (XPS) spectroscopies. FT-IR analysis of the cysCDs showed differences pertaining to their surface groups relative to the precursors (Fig. S8†). The cysCDs have characteristic bands indicative of O–H stretching vibrations at 3500 cm^{-1}, C=O stretching at 1700 cm^{-1} and C–O stretches at 1100 and 870 cm^{-1} that indicate carboxylic acid and other oxygen-containing functional groups, respectively, on the surface of the dots (Fig. 2b). The amino functional groups were also present in chiral CDs with bands at 3050–3250 cm^{-1} and 1510 cm^{-1} ascribed to the N–H and amide vibrations, respectively. The stretching vibrations of C–H, C=C and C–C are also noted in the FT-IR spectra at 2950, 1420 and 1330 cm^{-1}, respectively. The typically weak S–H stretch is not observed in the FT-IR spectrum, however, the S=O stretch can be observed at ~1100 cm^{-1}.

The FT-IR findings are further corroborated by the XPS results. The XPS survey scan of the cysCDs shows prominent peaks at 533.08, 401.08, 289.08 and 166.08 eV corresponding to oxygen (O 1s), nitrogen (N 1s), carbon (C 1s) and sulfur (S 2p) binding energies, respectively. High resolution scans of the O 1s state (Fig. 2c) shows the presence of C–OH/C–O–C and C=O functional groups with deconvoluted binding energies observed at 533.66 and 532.16 eV, respectively. The pyridinic, pyrrolic and graphitic N groups in the CDs can be observed in high resolution of N 1s spectrum with binding energies at 401.62, 400.53 and 400.08 eV (Fig. 2d). Moreover, the C 1s spectrum (Fig. 2e) showed binding energies at 285.26, 287.22 and 289.06 eV that can be attributed to the –C/C=C, C–N/C–S, and C=O functional groups present in the CDs. Finally, the presence of S=O and S–H groups in the CDs can be observed in the S 2p spectrum at 164.66 and 163.58 eV, respectively (Fig. 2f). Our chiral cysteine CDs evidence similar surface functional groups as reported in the literature.[33–38]

The effect of synthesis temperature

The synthesis temperature had a stark impact on the residual chirality of the dots as observed from the circular dichroism spectra of L-cysCDs (Fig. 3a).[48] As the reaction temperature increased, there was a drastic decrease in the residual chirality observed in the L-cysCDs at the same precursor ratio and synthesis time. It could be postulated that with an increase in synthesis temperature, there is a greater breakdown of chiral precursors and chiral moieties, essentially rendering the dots achiral. It is likely that at higher reaction temperatures, the fluorophores on the surface of the dots are carbonized. As such, the cysteine residues and their derivatives are preferentially incorporated into the core of the CDs at higher reaction temperatures leading to the observed decrease in the residual chirality of the nanoparticles. The breakdown of the cysteine residues and their derivatives on the surface of the nanoparticle could be estimated by the quantification of free thiols on the surface by Ellman's reagent. As the reaction temperature increased, the concentration of free thiols on the surface on the dots decreased with values of 0.019, 0.009, 0.008 and 0.008 mM at 160, 180, 200 and 220 °C, respectively (Table S3†).

Furthermore, XRD spectra of the cysCDs showed a disappearance of the sharp peaks with an increase in temperature indicating increasing disorder in the nanoparticle and a change in the structure of the cysCDs (Fig. S9†). The change was further supported by the differences in the TGA weight loss profile of the cysCDs as a function of increasing reaction temperatures (Fig. S10†). Thus, the variance in concentration of the surface thiols groups affirms the decrease in the residual chirality.

There were no significant differences in the optical and physical properties of the cysCDs reacted at the different temperatures. All cysCDs showed absorbance bands at ~250 nm and ~350 nm corresponding to $\pi \rightarrow \pi^*$ and $n \rightarrow \pi^*$ transitions and they exhibited fluorescence maxima at 420 nm (Fig. S11a†). Colloidal dispersions of cysCDs prepared at the same concentration revealed an increase in fluorescence intensity with increasing reaction temperatures (Fig. S11b†). We once again reason that at more elevated reaction temperatures there is a greater breakdown of precursors. This allowed for the formation of a well-hybridized network, enhancing the aromatic
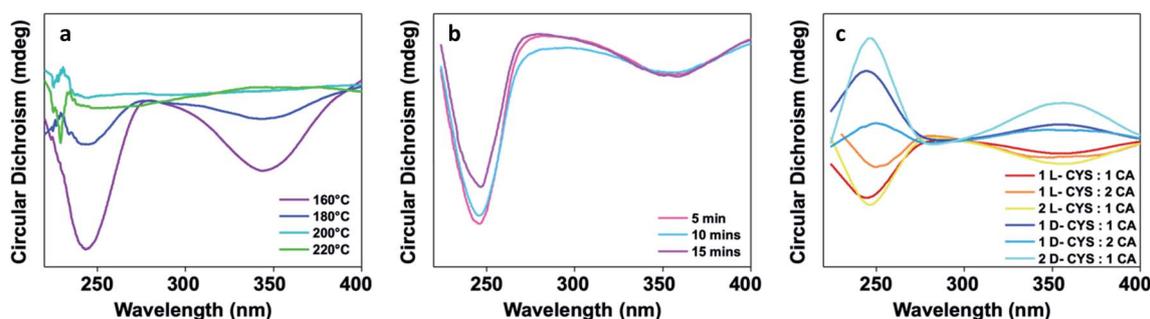

Fig. 3 Circular dichroism spectra of cysCDs prepared using different reactions parameters. (a) The circular dichroism spectra of L-cysCDs show a decrease in the chirality of the cysCDs with increasing reaction temperatures, (b) with an increase in reaction times at a reaction temperature of 160 °C, a decrease in residual chirality is observed most notably at 15 min, (c) an increase in the concentration of cysteine chiral precursor, relative to citric acid, during synthesis results in a stronger chiral signal while a decrease in the concentration of cysteine, decreases the chiral signal in the dots.

conjugated core and the associated fluorescence properties. FT-IR analysis of these cysCDs prepared at different reaction temperatures showed that the surface functional groups are relatively similar, which is expected as we noted that the precursors remained unchanged (Fig. S11c†).

Unpassivated carbon dots using citric acid were also synthesized at different reaction temperatures to gain a better understating of the chiro-optical properties of the cysCDs. These CDs absorbed at ~350 nm (Fig. S1a†); however, there were no significant luminescent (Fig. S1b†) nor chiral properties (Fig. S1c†) observed in these systems.

The effect of synthesis time

A similar decrease in chirality was noted as the reaction time is increased from 5 to 15 min at a reaction temperature of 160 °C (Fig. 3b). Reaction time appeared to have a more modest effect relative to the decrease observed from the variation of synthesis time. The prolonged reaction times favour the formation of a well-hybridized nanoparticle core at the expense of the surface groups. Hence, quantification of the free thiols on the surface of the dots was seen to decrease in value from 0.019 to 0.006 and 0.004 mM at reaction times of 5, 10 and 15 min, respectively (Table S3†). The cysCDs, prepared at various reaction times, were also investigated using XPS and the results also indicated a decrease in S–H and an increase in S=O with increasing reaction time (Fig. S12†). A subsequent increase in the C=C/C–C was also observed with longer synthesis times further supporting the formation of a hybridized core (Fig. S12†). The changes to the structure were also supported by XRD analyses, showing increasing amorphous nature and decreasing crystalline peaks (Fig. S13†). Moreover, the changes in the TGA weight loss profiles further indicated the change in the surface composition of the CDs (Fig. S14†). No significant differences were noted in the optical properties of cysCDs in comparison to their counterparts prepared at different times (Fig. S15a†). There was a similar trend of increasing fluorescence with time as with reaction temperature as a more hybridized core was formed (Fig. S15b†) and no significant change was observed in the functional groups present as shown by the FTIR (Fig. S15c†).

The effect of precursor ratios

The chirality of the dots was further tuned by altering precursor ratios at the optimized conditions of 160 °C and 10 min (Fig. 3c). As the ratio of the chiral cysteine to achiral citric acid is doubled (2 : 1), more prominent absorbance bands at 250 nm and 350 nm were observed in the circular dichroism spectra. As more chiral precursors are available, an increased residual chirality was observed because there was an abundance of chiral precursors that can contribute to the formation of the dots. Conversely, a decrease in the cysteine to citric acid ratio (1 : 2) showed a decrease in the absorbance of circularly polarized light by the dots at the same wavelengths since fewer chiral precursor molecules were available. Once again, titration using Ellman's reagent highlights the concentration of free thiols on the surface of the dots with more free thiols present (0.010 mM) in the 2 : 1 cysteine : citric acid ratio in comparison to 1 : 2

cysteine : citric acid ratio (0.006 mM, Table S3†). The XRD profile of these CDs showed a decrease in crystallinity with an increasing concentration of citric acid (Fig. S16†). The cyclization of citric acid with amines and amino containing groups such as those found in cysteine leads to hybridized networks and a lack of surface functional groups. Furthermore, the change in the cysCD surface can be observed by the variation in the TGA profiles (Fig. S17†). There were no significant differences observed in the optical properties of the cysCDs as previously noted for the other reaction parameters (Fig. S18a†). The fluorescence of the cysCDs does however increase as a function of increasing cysteine precursor used (Fig. S18b†) and once again the FT-IR analysis indicates similar functional groups on the surface of these CDs (Fig. S18c†).

The antimicrobial effect of the chiral CDs

Antibiotic resistance is a growing and imminent threat affecting human morbidity and mortality.[49] The development of novel antimicrobial drugs is crucial to combat resistant infectious disease.[50] Nanoparticles have been reported to have antibacterial activity[50,51] and recently, chiral nanoparticles have been tested for antibacterial activity.[52] We have tested L- and D-cysCDs (1 : 1 ratio) for antimicrobial activity through MIC determination on Gram-positive and Gram-negative bacteria using 96-well plates and agar broth dilutions. The Gram-positive strains tested were *Bacillus subtilis* DSM10, *Burkholderia thailandensis* E264, and *Micrococcus luteus* DSM20030. The Gram-negative strains tested were *E. coli* ATCC 25922 and MG1655, as well as *Klebsiella aerogenes* ATCC 13048. The concentration range of cysCDs used ranged from 15.6 μg mL^{-1} to 8 mg mL^{-1} with 2-fold increments from well to well, following standard broth microdilution guidelines.[39] The concentration range of cysCDs used ranged from 62.5 μg mL^{-1} to 4 mg mL^{-1} for the agar broth dilutions protocol (Fig. 4).[40]

CD concentrations ranging from 0.25–4 mg mL^{-1} were required to inhibit bacterial growth, varying by both the strain tested and the chirality of the cysCDs (Table 1). The MIC of L-cysCDs on *B. subtilis*, *M. luteus* and *B. thailandensis* was determined to be 4 mg mL^{-1}, 2 mg mL^{-1} and 1 mg mL^{-1}, respectively (Table 1). On the other hand, the MIC of D-cysCDs was determined to be 0.5–1 mg mL^{-1} for all Gram-positive strains (Table 1). L-cysCDs inhibited the growth of the Gram-negative bacteria *E. coli* at 4 mg mL^{-1} in both liquid culture and when impregnated into agar plates, while D-cysCDs had an MIC of 2 mg mL^{-1} in both liquid and plate culture (Table 1, Fig. 4).[40] For *K. aerogenes*, inhibition with L-cysCDs was achieved at 0.25 mg mL^{-1} and at 1 mg mL^{-1} with D-cysCDs (Table 1).

The difference in MICs between L- and D-cysCDs suggests that stereochemistry has a role in the inhibitory function of cysCDs. The chemical and physical composition of the chiral cysCDs are similar to each other as suggested by the FT-IR, TEM, UV-Vis and fluorescence spectroscopies with the major difference stemming from the chirality of the nanoparticles. The cysCDs behave differently in chiral environments as suggested by the interaction of the CDs with circularly polarized light. It is known that enantiomeric molecules often interact
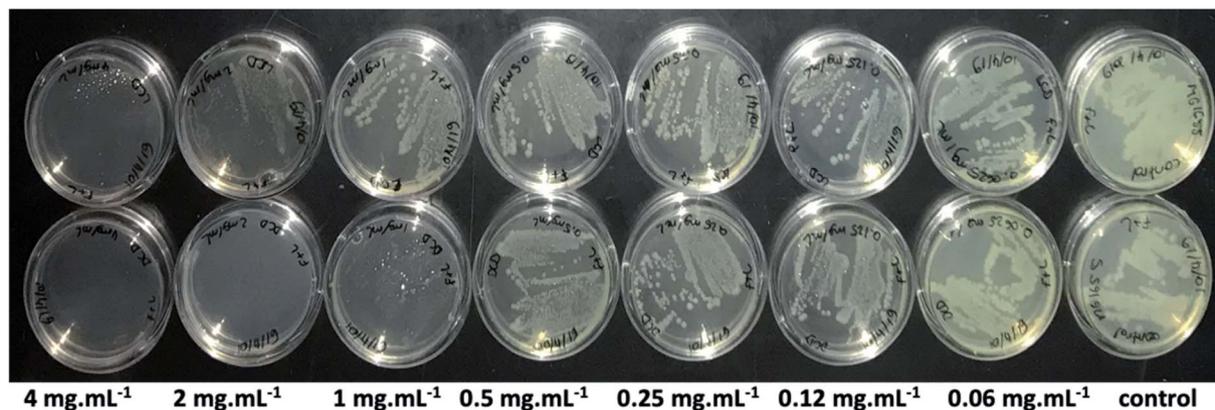
Fig. 4 The anti-bacterial properties of chiral cysCDs (1 : 1 ratio). The top row (from left to right) exhibits the antibacterial property of L-cysCDs at decreasing concentration inhibiting *E. coli* (MG 1655) growth at an optimal concentration of 4 mg mL^{-1}. The bottom row (from left to right) exhibits the antibacterial property of D-cysCDs at decreasing concentration inhibiting *E. coli* growth at an optimal concentration of 2 mg mL^{-1}.

Table 1 MIC data of exposure of L-cysCD and D-cysCD on 6 bacterial strains

Bacterial strain	MIC L-cysCDs (mg mL^{-1})	MIC D-cysCDs (mg mL^{-1})
M. luteus DSM20030	2	0.5
B. subtilis DSM10	4	1
B. thailandensis E264	1	1
K. aerogenes ATCC 13048	0.25	1
E. coli ATCC 25922	4	2
E. coli MG1655	4	2

differently within biological systems due to their stereospecific nature. Furthermore, similar anti-microbial behaviour was also noted by the chiral cysCDs between liquid and solid media, as such they could be useful in the incorporation to smart surfaces, strip tests, potential biological sensors, *etc.*

Previous studies have attempted to explain the mechanism of action of nanoparticles for antimicrobial activity through the generation of reactive oxygen species (ROS) causing DNA damage and oxidation of proteins in bacterial cells.[50] To determine if chiral cysCDs generated similar ROS we conducted a peroxide strip test assay. The test was negative, suggesting that the growth inhibition we see is not due to ROS production. Alternatively, the stereoselective effect of the nanoparticles discussed earlier can be explained by specific interactions with intracellular proteins, which could inhibit bacterial growth.

Conclusions

In conclusion, the residual chirality of cysCDs could be tuned by variation of reaction parameters including reaction temperature, time and precursor concentrations. Chiral cysCDs were successfully synthesized from L- and D-cysteine enantiomers with citric acid using a facile microwave synthesis. Reaction temperatures showed the greatest impact on the residual chiral

signal observed in the dots with a decrease in the chirality as the reaction temperature increased. This was attributed to the decomposition of the chiral precursors and derivatives to form a more hybridized core. Similarly, an increase in the reaction time also decreased the chiral signal from the dots. A significant change in chirality was observed from the chiral precursor ratios used to synthesize the cysCDs since an increased concentration of L- or D-cysteine during synthesis offered a greater potential for incorporation of the chiral precursor. The D-cysCDs demonstrated anti-microbial activity in common bacterial strains, at lower MICs compared to their L-counterparts, indicating that the stereochemistry of the dots has an effect on their biological activity. The concentration of D-cysCDs was at least 2-fold lower than L-cysCDs to observe similar bacterial growth inhibition except for *K. aerogenes* ATCC 13048. Furthermore, the inhibition was observed in both solid and liquid media opening up possibilities for applications in chiral antibacterial films and surfaces.

Conflicts of interest

There are no conflicts to declare.

Acknowledgements

Shang. We would also thank our undergraduate researcher Tolotriniaina Randriamialison for his help throughout the project.

Notes and references

1 A. W. Schwartz, *Curr. Biol.*, 1994, **4**, 758–760.
2 L. A. Nguyen, H. He and C. Pham-Huy, *Int. J. Biomed. Sci.*, 2006, **2**, 85–100.
3 J. S. Millership and A. Fitzpatrick, *Chirality*, 1993, **5**, 573–576.
4 R. Crossley, *Chirality and Biological Activity of Drugs*, 1995, vol. 7.
5 C. Gautier and T. Bürgi, *J. Am. Chem. Soc.*, 2006, **128**, 11079–11087.
6 J. K. Gansel, M. Thiel, M. S. Rill, M. Decker, K. Bade, V. Saile, G. von Freymann, S. Linden and M. Wegener, *Sci. 80*, 2009, **325**, 1513–1515.
7 C. Song, M. G. Blaber, G. Zhao, P. Zhang, H. C. Fry, G. C. Schatz and N. L. Rosi, *Nano Lett.*, 2013, **13**, 3256–3261.
8 A. Azizi, B. Ranjbar, T. T. Moghadam and Z. Bagheri, *Plasmonics*, 2014, **9**, 273–281.
9 T. Nakashima, Y. Kobayashi and T. Kawai, *J. Am. Chem. Soc.*, 2009, **131**, 10342–10343.
10 J. K. Choi, B. E. Haynie, U. Tohgha, L. Pap, K. W. Elliott, B. M. Leonard, S. V. Dzyuba, K. Varga, J. Kubelka and M. Balaz, *ACS Nano*, 2016, **10**, 3809–3815.
11 J. Yeom, B. Yeom, H. Chan, K. W. Smith, S. Dominguez-Medina, J. H. Bahng, G. Zhao, W. S. Chang, S. J. Chang, A. Chuvilin, D. Melnikau, A. L. Rogach, P. Zhang, S. Link, P. Král and N. A. Kotov, *Nat. Mater.*, 2015, **14**, 66–72.
12 Y. Zhou, R. L. Marson, G. Van Anders, J. Zhu, G. Ma, P. Ercius, K. Sun, B. Yeom, S. C. Glotzer and N. A. Kotov, *ACS Nano*, 2016, **10**, 3248–3256.
13 U. Tohgha, K. K. Deol, A. G. Porter, S. G. Bartko, J. K. Choi, B. M. Leonard, K. Varga, J. Kubelka, G. Muller and M. Balaz, *ACS Nano*, 2013, **7**, 11094–11102.
14 J. Wang, W. Wang, P. Sun, Z. Yuan, B. Li, Q. Jin, D. Ding and T. Chen, *J. Mater. Chem.*, 2006, **16**, 4117–4122.
15 H. Qiu, S. Wang, W. Zhang, K. Sakamoto, O. Terasaki, Y. Inoue and S. Che, *J. Phys. Chem. C*, 2008, **112**, 1871–1877.
16 Y. Han, L. Zhao and J. Y. Ying, *Adv. Mater.*, 2007, **19**, 2454–2459.
17 A. Nelson, *Letters to Nature*, 2012, **429**, 253–262.
18 S. Zhong, H. Cui, Z. Chen, K. L. Wooley and D. J. Pochan, *Soft Matter*, 2007, **4**, 90–93.
19 R. M. Ho, Y. W. Chiang, C. C. Tsai, C. C. Lin, B. T. Ko and B. H. Huang, *J. Am. Chem. Soc.*, 2004, **126**, 2704–2705.
20 J. Dupont, G. Liu, K. I. Niihara, R. Kimoto and H. Jinnai, *Angew. Chem., Int. Ed.*, 2009, **48**, 6144–6147.
21 E. E. Maroto, M. Izquierdo, S. Reboredo, J. Marco-Martínez, S. Filippone and N. Martín, *Acc. Chem. Res.*, 2014, **47**, 2660–2670.
22 R. Jasti and C. R. Bertozzi, *Chem. Phys. Lett.*, 2010, **494**, 1–7.
23 W. Ruland, A. K. Schaper, H. Hou and A. Greiner, *Carbon*, 2003, **41**, 423–427.

24 J. R. Sanchez-Valencia, T. Dienel, O. Gröning, I. Shorubalko, A. Mueller, M. Jansen, K. Amsharov, P. Ruffieux and R. Fasel, *Nature*, 2014, **512**, 61–64.
25 N. Suzuki, Y. Wang, P. Elvati, Z. B. Qu, K. Kim, S. Jiang, E. Baumeister, J. Lee, B. Yeom, J. H. Bahng, J. Lee, A. Violi and N. A. Kotov, *ACS Nano*, 2016, **10**, 1744–1755.
26 M. Vázquez-Nakagawa, L. Rodríguez-Pérez, M. A. Herranz and N. Martín, *Chem. Commun.*, 2016, **52**, 665–668.
27 Y. Yu, W. Liu, J. Ma, Y. Tao, Y. Qin and Y. Kong, *RSC Adv.*, 2016, **6**, 84127–84132.
28 V. Mishra, A. Patil, S. Thakur and P. Kesharwani, *Drug Discovery Today*, 2018, **23**, 1219–1232.
29 R. Das, R. Bandyopadhyay and P. Pramanik, *Mater. Today Chem.*, 2018, **8**, 96–109.
30 Y. P. Sun, B. Zhou, Y. Lin, W. Wang, K. A. S. Fernando, P. Pathak, M. J. Meziani, B. A. Harruff, X. Wang, H. Wang, P. G. Luo, H. Yang, M. E. Kose, B. Chen, L. M. Veca and S. Y. Xie, *J. Am. Chem. Soc.*, 2006, **128**, 7756–7757.
31 Y. Wang and A. Hu, *J. Mater. Chem. C*, 2014, **2**, 6921.
32 S. Y. Lim, W. Shen and Z. Gao, *Chem. Soc. Rev.*, 2014, **44**, 362–381.
33 A. Ghosh, B. Parasar, T. Bhattacharyya and J. Dash, *Chem. Commun.*, 2016, **52**, 11159–11162.
34 Y. Zhang, L. Hu, Y. Sun, C. Zhu, R. Li, N. Liu, H. Huang, Y. Liu, C. Huang and Z. Kang, *RSC Adv.*, 2016, **6**, 59956–59960.
35 M. J. Deka and D. Chowdhury, *RSC Adv.*, 2017, 7, 53057–53063.
36 L. Hu, H. Li, C. Liu, Y. Song, M. Zhang, H. Huang, Y. Liu and Z. Kang, *Nanoscale*, 2018, **10**, 2333–2340.
37 F. Li, Y. Li, X. Yang, X. Han, Y. Jiao, T. Wei, D. Yang, H. Xu and G. Nie, *Angew. Chem., Int. Ed.*, 2018, **57**, 2377–2382.
38 M. Zhang, L. Hu, H. Wang, Y. Song, Y. Liu, H. Li, M. Shao, H. Huang and Z. Kang, *Nanoscale*, 2018, **10**, 12734–12742.
39 CLSI, in *Performance Standards for Antimicrobial Susceptibility Testing*, Clinical and Laboratory Standard Institute, Wayne, PA, 29th edn, 2019.
40 CLSI, in *Methods for Dilution Antimicrobial Susceptibility Tests for Bacteria That Grow Aerobically*, Clinical and Laboratory Standard Institute, Wayne, PA, 11th edn, 2018.
41 L. Shi, J. H. Yang, H. B. Zeng, Y. M. Chen, S. C. Yang, C. Wu, H. Zeng, O. Yoshihito and Q. Zhang, *Nanoscale*, 2016, **8**, 14374–14378.
42 J. Schneider, C. J. Reckmeier, Y. Xiong, M. Von Seckendorff, A. S. Susha, P. Kasak and A. L. Rogach, *J. Phys. Chem. C*, 2017, **121**, 2014–2022.
43 T. N. J. I. Edison, R. Atchudan, M. G. Sethuraman, J. J. Shim and Y. R. Lee, *J. Photochem. Photobiol., B*, 2016, **161**, 154–161.
44 J. Dore, A. Burian and S. Tomita, *Acta Phys. Pol., A*, 2000, **98**, 495–504.
45 Z. Lin, M. K. Song, Y. Ding, Y. Liu, M. Liu and C. P. Wong, *Phys. Chem. Chem. Phys.*, 2012, **14**, 3381–3387.
46 J. Kumar, K. G. Thomas and L. M. Liz-Marzán, *Chem. Commun.*, 2016, **52**, 12555–12569.
47 S. S. Zhang, *Energies*, 2014, **7**, 4588–4600.

48 N. Li, Z. Wang and Z. Shi, *Synthesis of Graphenes with Arc-Discharge Method*, INTECH Open Access Publisher, Shanghai, 2011, ch. 2, pp. 23–39, ISBN: 978-953-307-217-3.

49 B. Aslam, W. Wang, M. I. Arshad, M. Khurshid, S. Muzammil, M. H. Rasool, M. A. Nisar, R. F. Alvi, M. A. Aslam, M. U. Qamar, M. K. F. Salamat and Z. Baloch, *Infect. Drug Resist.*, 2018, **11**, 1645–1658.

50 F. Lin, Y.-W. Bao and F.-G. Wu, *C*, 2019, **5**, 33.

51 A. Khezerlou, M. Alizadeh-Sani, M. Azizi-Lalabadi and A. Ehsani, *Microb. Pathog.*, 2018, **123**, 505–526.

52 Q. Xin, Q. Liu, L. Geng, Q. Fang and J. R. Gong, *Adv. Healthcare Mater.*, 2017, **6**, 1601011.